

Article

Load Frequency Control of Marine Microgrid System Integrated with Renewable Energy Sources

Guoqiang Zhang ¹, Irfan Ahmed Khan ², Amil Daraz ^{1,3,*}, Abdul Basit ^{1,3} and Muhammad Irshad Khan ⁴

¹ School of Information Science and Engineering, NingboTech University, Ningbo 315100, China

² Department of Electrical Engineering, Faculty of Engineering, Universiti Malaya, Kuala Lumpur 50603, Malaysia

³ College of Information Science and Electronic Engineering, Zhejiang University, Hangzhou 310027, China

⁴ College of Electronics and Information Engineering, Nanjing University of Aeronautics and Astronautics (NUAA), Nanjing 210000, China

* Correspondence: amil.daraz@nbt.edu.cn

Abstract: In seaports, low-carbon energy systems and energy efficiency have become increasingly important as a result of the evolution of environmental and climate change challenges. In order to ensure the continued success of seaports, technological advancements must be introduced to a number of systems, such as seaport vehicles, harbor cranes, and the power sources of berthed ships. Harbor areas might need a microgrid to handle these aspects. Typically, microgrids that substitute conventional generator units with renewable energy sources (RES) suffer from system inertia problems, which adversely affect microgrid frequency stability. A load frequency controller (LFC) based on a novel modified proportional integral derivative with filter (MPIDF) is presented in this paper for enhancing the performance of marine microgrid system (MMS). The serval optimization algorithm (SOA), a recent bio-inspired optimization algorithm, is used to optimize the MPIDF controller coefficients. This controller is tested on a marine microgrid containing a number of RES such as wind turbine generators, sea wave energy, and solar generation. The efficacy of the proposed MPIDF controller is verified with respect to other controllers such as PIDF and PI. Similarly, the proposed meta-heuristic algorithm is validated as compared to other algorithms including particle swarm optimization (PSO), ant colony optimization (ACO), and jellyfish swarm optimization (JSO). This study also evaluates the robustness of the proposed controller to different perturbations in step load, changes in system parameters, and other parameter variations.

Keywords: marine microgrid; load frequency control; PID controller; renewable energy sources; serval optimization algorithm; optimization



Citation: Zhang, G.; Khan, I.A.; Daraz, A.; Basit, A.; Khan, M.I. Load Frequency Control of Marine Microgrid System Integrated with Renewable Energy Sources. *J. Mar. Sci. Eng.* **2023**, *11*, 844. <https://doi.org/10.3390/jmse11040844>

Academic Editor: Yassine Amirat

Received: 20 March 2023

Revised: 7 April 2023

Accepted: 11 April 2023

Published: 17 April 2023



Copyright: © 2023 by the authors. Licensee MDPI, Basel, Switzerland. This article is an open access article distributed under the terms and conditions of the Creative Commons Attribution (CC BY) license (<https://creativecommons.org/licenses/by/4.0/>).

1. Introduction

The evolution of environmental and climate change concerns has made low-carbon energy systems and clean energy more crucial at seaports. A number of systems—including seaport vehicles, harbor cranes, and the power source of berthed ships—must be upgraded technologically in order to assure the seaport’s continuous prosperity. The harbor area may require the establishment of a microgrid to address these aspects. The development of microgrids, mostly for domestic use, has been widespread on the mainland and islands. As a result, their development in such places faces several challenges, including high power requirements and the managing and monitoring of a wide range of loads [1]. Generally, difficulties with system inertia impair the frequency stability of microgrids in which renewable energy sources (RES) including sea wave energy (SWE), Photovoltaic (PV), and wind turbines (WTs) replace conventional generator units. Vessels that use this technology can reduce pollution, improve stability, and boost energy efficiency [2].

Maritime power systems that use wind turbine generators, SWE, photovoltaics (PV), and ESSs are classified as a form of movable island—MG. As a result, a wide range of studies

have been undertaken in this sector; for example, in [3], a hybrid photovoltaic, battery, and diesel vessel power system was examined. As a result, the impact of sea transportation is not considered in this paper. The authors described a feasibility analysis for the tidal energy used in [4]; notwithstanding frequency stability issues, the assimilation of tidal and wind power units to a power system grid was investigated. The authors of [5] utilized lithium-ion batteries in conjunction with diesel generators for ship crane operations. The authors presented a thorough study on the active performance of stall and pitch standardized tidal turbines in [6]. Furthermore, Reference [7] discusses the economic and environmental benefits of hybrid diesel–photovoltaic (PV) systems with an ESS. Reference [8] investigates the stability of hybrid diesel–battery–PV vessel power systems. The authors of [9] developed a multi-objective optimization approach in PV–diesel hybrid PS to address the sizing problem. A mixed integer linear programming model proposed by Iris and Lam [10] has been applied to the problem of planning and managing seaport operations together with energy management in the context of smart grids, while taking into account the uncertain generation of renewable energy. The authors of [11] proposed an interval-iterative approach for efficient RES distribution in a diesel/PV/RES-based ship PS. The impact of integrating a tidal power unit on a real-world grid was examined in [12]. The authors of [13] showed maximum power-point tracking at various tidal speeds. Wave energy shows a great capability for contributing to the goal of complete energy generation by renewable energies; it can meet more than 10% of total world electricity consumption [14]. The authors of [15] illustrated the formation of the Archimedes wave shift, which was modelled as an unmanageable generation system in this work. In [16], the authors describe the design and implementation of a monitoring system utilizing Internet of things technology for a lithium-ion battery integrated into a hybrid microgrid.

A simple proportional integral derivative (PID) and PI controller was used in the LFC design due to its simplicity [17,18]. For instance, to enhance the frequency response under various load disturbances, Ref. [19] proposed a PI-LFC-based particle swarm optimization (PSO) technique. In the presence of WT and PV, Alayi et al. [20] employed a PID controller as a secondary regulator to stabilize the microgrid's frequency in island mode. A microgrid system that employed battery and pump-hydro storage systems was examined by the authors in [21] in order to analyze the frequency and power balance. Additionally, various optimization algorithms—including the fitness dependent optimizer (FDO) [22], ant colony optimization (ACO) [23], volleyball premier league algorithm (VPLA) [24], Fox optimizer algorithm (FOA) [25], salp swarm algorithm (SSA) [26], whale optimization algorithm (WOA) [27], improved fitness dependent optimizer (IFDO) [28], social-spider optimizer (SSO) [29], Jaya intelligent algorithm [30], Jellyfish Search Optimizer (JSO) [31], Antlion optimization (ALO) [32], PSO algorithm [33], and hybridization of sine cosine algorithm (SCA) with FDO [34] techniques—have been used to tune controller parameters. Additionally, some authors have introduced fractional-order PID controllers to address the LFC issue in multi-region units. As part of the PIDF controller, a low-pass filter can be added to the derivative coefficient of the PID controller to further enhance the dynamics of the system. As a result of the filter, it is possible to reduce the amount of undesirable high-frequency noise present in the control signal [35,36]. Furthermore, some researchers have also recommended using fractional and tilt order controllers in addition to traditional controllers in order to improve the performance of systems [37,38].

The previously stated control strategies have been applied to traditional production units with high-order inertia. Furthermore, most of these strategies do not account for the short-term frequency equilibration provided by intermittent RES. The maritime MG, meanwhile, is a low-inertia system that depends on irregular RES. For traditional microgrids and conventional power systems, a number of control strategies have been put forward to address the LFC problem; however, marine/shipboard microgrids have received very little attention. Consequently, the contribution of this paper is emphasized in this study.

- Various renewable energy resources have been considered for marine microgrids—including sea wave energy (SWE), wind turbine generators (WTGs), and solar generation system.
- Various generation sources have been implemented with communication time-delay nonlinearity to increase the PS's practicality and realism.
- In order to develop a marine microgrid based on renewable and sustainable energy sources, a novel, improved PIDF controller called the I-PDF controller was developed and implemented.
- A modified PIDF controller was compared with other conventional controllers, such as PIDF and PI.
- The coefficient of the proposed I-PDF controller was optimized with a novel meta-heuristic algorithm known as the serval optimization algorithm (SOA). Other algorithms such as the jellyfish swarm algorithm (JSO), particle swarm optimization (PSO), and ant colony optimization (ACO) were used to verify the SOA's effectiveness.
- In the proposed diverse renewable energy source-based marine microgrid, multi objective functions of the integral time square error, integral time absolute error, and integral square error were formulated.
- To demonstrate the robustness of the proposed frequency control technique, sensitivity testing of the SOA-adjusted I-PDF controller was conducted under uncertain parametric variables such as the droop factor (R), Photovoltaic gain (KPV), and loading conditions.

This work is structured as follows: Section 2 deals with marine microgrid modelling, followed by subsections on wind turbines, sea wave energy, and photovoltaics. Serval optimization algorithms are presented in Section 3, whereas controller structures and objective functions are presented in Section 4. In Section 5, the results and implementation are discussed, whereas Section 6 concludes the presented research with future directions.

2. Marine Microgrid Modelling

This section provides a detailed structural schematic analysis of the proposed marine microgrid system, as shown in Figure 1. The suggested marine MG model is made up of wind turbine generators (WTGs), SWE, and solar power generation (SPG). A full description of the proposed renewable power-based marine microgrid system is presented in the following subsection.

2.1. Modelling of Wind Turbine Generation

Traditionally, electricity is generated using wind turbines (WT). A WT's output of automated power is typically affected by the attributes of the turbine and the wind speed. It has been shown [39] that the following equation can be used to describe a wind turbine's output:

$$p = \frac{1}{2} A \rho_A C_p V^3 \quad (1)$$

$$A = \pi R^2 \quad (2)$$

$$A = 2hR \quad (3)$$

where A represents the area for horizontal and vertical turbines, h is the height, V is the wind speed, R is the radius, C_p is the power coefficient, and ρ_A is the air density. The following formulas can be used to calculate the WT's torque.

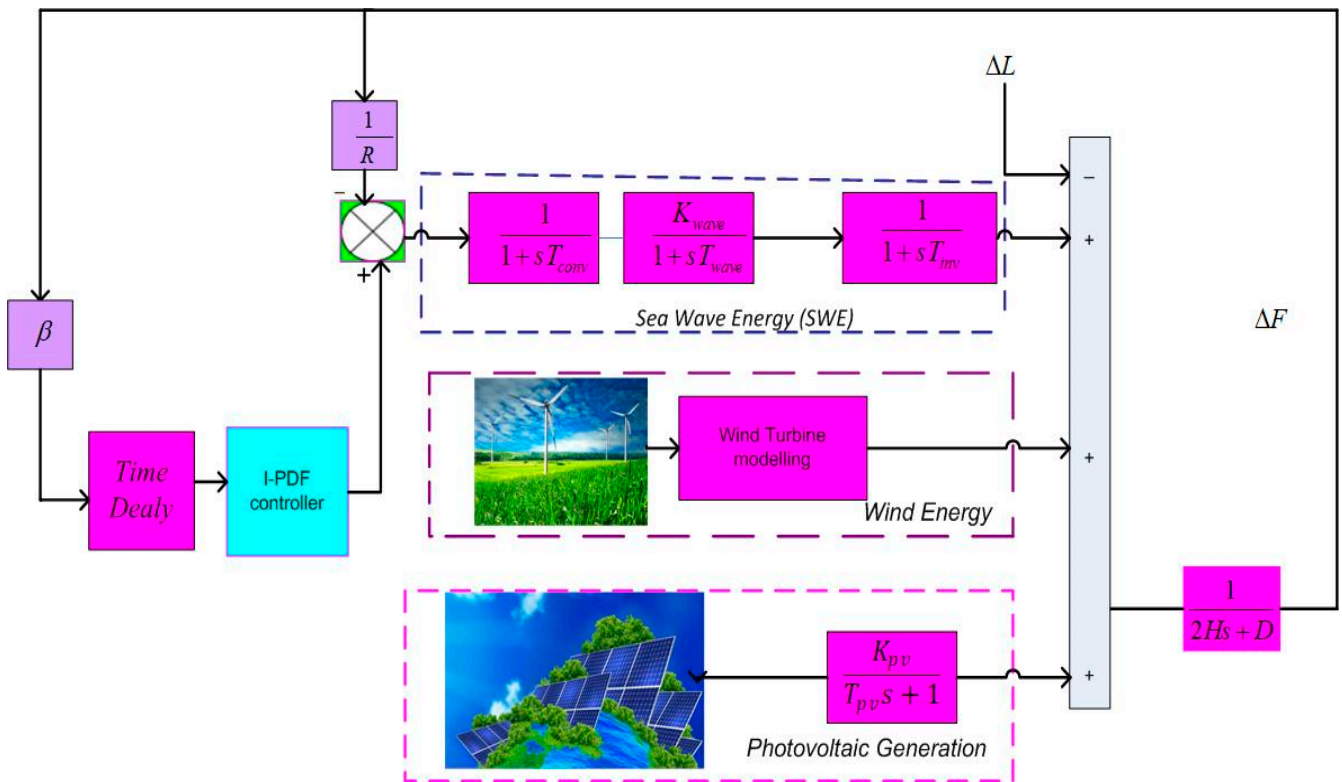


Figure 1. Modelling of marine microgrid system.

$$T_T = \frac{P}{\omega} = \frac{\rho_A A C_p V^3}{2\omega} = \frac{\rho_A A C_p V^3}{2\lambda^3} \omega^2 \tag{4}$$

$$T_G = \frac{\rho_A A C_p^{Max} V^3}{2\lambda_E^3} \omega^2 \tag{5}$$

where C_p^{Max} is the maximum extent of the power constant and (λ_E^3) represents the tip speed ratio. The power number (N_p) can be expressed as follows, which is based on the Reynolds number (Re) and type of impeller [39]:

$$N_p = \frac{P_g}{\rho_w n^3 d^5} \tag{6}$$

where ρ_w is the liquid’s density, P is the energy supplied by the WT, g is the gravitational force, d is the impeller’s diameter, and n is the blade’s speed. The Reynolds number is expressed as follows:

$$Re = \frac{\rho_w n d^2}{\mu} \tag{7}$$

where μ denotes the viscosity of the liquid. The relationship between the Reynolds number (Re) and power number (N_p) for both types of flow is given by [39]:

$$N_p = B Re^z \tag{8}$$

$$B = \frac{P_g}{\rho_w n^3 d^5} \tag{9}$$

There is a quadratic relationship between the torque and load, and it can be expressed as follows:

$$T_G = \frac{\rho_w B d^5}{8\pi^3 g} \omega^2 \tag{10}$$

$$\frac{\rho_A A C_p^{Max} R^3}{2\lambda_E^3} = \frac{\rho_w B d^5}{8\pi^3 g} \tag{11}$$

The diameter of the impeller can be determined as follows:

$$d = \left(\frac{4\pi^3 g \rho_A A C_p^{Max} R^3}{\rho_w B \lambda_E^3} \right)^{0.2} \tag{12}$$

The wind heat generator increases the temperature of the fluid used for heat transfer by transforming mechanical energy into heat. Under lossless conditions, the energy given by the WT to the heat generator determines the increase in fluid temperature, which can be expressed as [39]:

$$\Delta T = \frac{1}{cm} \int P dt \tag{13}$$

where c represents the specific heat and m is the mass of the fluid. The mechanical system of a WT with a heat generator is described by the equation below:

$$J_T + J_G \left(\frac{d\omega}{dt} \right) = T_T - T_G \tag{14}$$

where T_T is the torque yielded by the WT, J_T is the WT's inertia, J_G is the heat generator's inertia, and T_G is the heat generator's load torque. Figure 2 depicts a schematic diagram of a wind turbine generator.

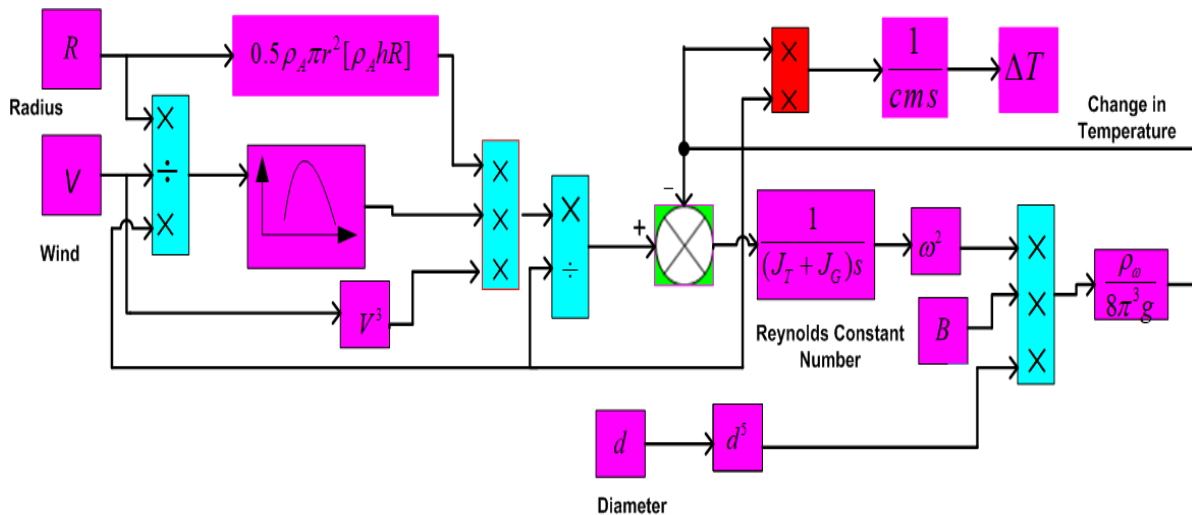


Figure 2. Wind turbine in a Marine Microgrid system.

2.2. Modelling of Sea Wave Energy (SWE)

Wave power will be generated by a permanent magnet synchronous generator. The subsequent calculations describe the system's dynamics using force (F_w) and velocity (V_w) [40,41]:

$$V_w = \frac{dx}{dt} \tag{15}$$

$$F_w = m_{ft} \frac{dV_w}{dt} + K_c x + (\beta_G + \beta_W) V_w \tag{16}$$

where m_{ft} is the total mass, x is the displacement of the floater and translator, β_G is the generator's constant damper, and β_W is the restriction of the wave swing. As a first-order converter, first-order generator, and first-order inverter, the system is modelled in Equation (17) [40]:

$$G_{wave} = \frac{1}{1 + sT_{conv}} \frac{K_{wave}}{1 + sT_{wave}} \frac{1}{1 + sT_{inv}} \tag{17}$$

where G_{wave} is the TF of the wave energy, T_{inv} and T_{conv} are the time constants of the inverter and converter, respectively, T_{wave} is the time constant, and K_{wave} is the gain constant.

2.3. Modelling of Photovoltaic Generation

Semiconducting material makes up Photovoltaic (PV) cells, which can convert photon energy directly into electricity. In addition, series and parallel resistors are used to model power loss in order to take border and external contacts, leakage current, and other factors into account. Due to the unpredictable nature of PV power generation, the behavior of PV can be represented by a random power supply. The TF of a solar system is shown by Equation (18) [41]:

$$G_{PVG} = \left(\frac{K_{pv}}{T_{pv}s + 1} \right) \tag{18}$$

where T_{pv} and K_{pv} are the time and gain constant, respectively.

3. Serval Optimization Algorithm (SOA)

A serval optimization algorithm (SOA) was developed by the authors of [42], which aimed to reproduce biological actions similar to those performed by servals in nature. Based on the serval's chasing tactic, the SOA mimics the hunting process in which prey is attacked and then hunted. There are two phases in the process of SOA implementation that are mathematically represented as exploitation and exploration. This analysis intends to evaluate the SOA's ability to solve optimization problems through the optimization of 39 standard benchmark functions from CEC's 2017 and 2019 test suites in order to evaluate its efficiency. To evaluate further, the proposed SOA approach is compared to the performance of 12 well-known optimization algorithms. In nature, the strategy of the serval during hunting is one of its most distinctive characteristics. A metaheuristic algorithm can be designed based on this intelligent process. The strategy of serval hunting is modelled in the SOA's layout, which is considered in the following section.

3.1. Initialization

By utilizing the search capabilities of its pursuit agents, the suggested SOA methodology is an inhabitant-based optimizer that can offer suitable solutions for optimization problems. The methodology utilized by wild servals that hunt for prey in the wild is like that used by search agents to find the best solution for a given problem. Servals compose the SOA population from a mathematical perspective to find the best solution in the search space. Thus, each of the servals represents a potential solution to the problem, and the value of the decision variables depends on its location. Servals are vectors from a mathematical perspective and the SOA population matrix—which can be represented using Equation (19). Equation (20) is used to generate a random position for the servals in the seek place at the start of the algorithm's implementation.

$$X = \begin{bmatrix} X_1 \\ \vdots \\ X_i \\ \vdots \\ X_N \end{bmatrix}_{N \times d} = \begin{bmatrix} x_{1,1} & \cdots & x_{1,i} & \cdots & x_{1,d} \\ \vdots & \ddots & \vdots & \ddots & \vdots \\ x_{i,1} & \cdots & x_{i,j} & \cdots & x_{i,d} \\ \vdots & \ddots & \vdots & \ddots & \vdots \\ x_{N,1} & \cdots & x_{N,j} & \cdots & x_{N,d} \end{bmatrix}_{N \times d} \tag{19}$$

$$x_{i,j} = lb_j + r.(ub_j - lb_j), i = 1, 2, 3 \dots \dots N, J = 1, 2, \dots, d \tag{20}$$

where, d represents the decision variables, N indicates the number of servals, r belongs to a random number in the limit $[0, 1]$, and ub_j and lb_j are the upper and lower limits of the j th decision variable, respectively. There is a population matrix of various locations denoted by X . Since each decision variable represents a potential solution, the suggested values of each approach can be used to assess the cost function of the problem. According to Equation (21), the cost function values can then be represented by a vector [42].

$$F = \begin{bmatrix} F_1 \\ \vdots \\ F_i \\ \vdots \\ F_N \end{bmatrix}_{N \times 1} = \begin{bmatrix} F(X_1) \\ \vdots \\ F(X_i) \\ \vdots \\ F(X_N) \end{bmatrix}_{N \times 1} \tag{21}$$

where F is the cost functions' vector. The optimal value among the computed values for the fitness function is chosen as the finest optimal solution, and the population participant pertaining to it is chosen as the best one. Considering that each SOA iteration updates the positions of all members of the population, it would seem that the best member should also be updated with the latest positions.

3.2. Mathematical Representation of SOA

Two phases that mimic the serval chasing tactic in life are used to update the SOA elements of the population in the search space. These stages are meant to simulate global search exploration and local search exploitation in SOA design.

3.2.1. Phase 1: (Exploration) Selection of Prey and Attacking

Servals are effective predators that utilize their excellent hearing skills to locate and attack their prey. The roles of servals are updated in the first phase of the SOA established on the computation of these approaches. The update triggers significant changes to the location of servals and results in a thorough search. The aim of this phase is to enhance the SOA exploration power in global searches as well as identifying the primary optimal region based on the SOA results. The position of the inhabitant's best partner is deemed the target location in the SOA design. First, the serval's new position is computed utilizing Equation (22) to simulate the serval's assault on the target. If the new role enhances the fitness values, it substitutes the prior serval position, as shown in Equation (23).

$$x_{i,j}^{P1} = x_{i,j} + r_{i,j}.(P_j - I_{i,j} \cdot x_{i,j}) \quad i = 1, 2, 3 \dots \dots N, \quad J = 1, 2, \dots, d \tag{22}$$

$$X_i = \begin{cases} X_i^{P1}, & F_i^{P1} < F_i; \\ X_i, & \text{Otherwise} \end{cases} \tag{23}$$

where $x_{i,j}^{P1}$ signifies the updated position, $I_{i,j}$ are numbers taken at random from the set of $\{1, 2\}$, F_i^{P1} is the objective function values, P denotes the prey location, and $r_{i,j}$ are random numbers $\in [0, 1]$.

3.2.2. Phase 2: (Exploitation) Chase Process

Servals engage in a chase process after targeting their prey in order to stop them before killing and devouring them. SOA uses this tactic in the second phase to update its population position. The serval positions in the search space are slightly altered by the model of the chase activity. In actuality, the goal of this SOA phase is to improve local search and increase the SOA's exploitation power. Equation (24) is used to calculate a recent arbitrary position close to the serval to accurately model the pursuit of the prey.

Equation (25) states that this new position of the corresponding serval replaces the previous one if it increases the value of the cost function.

$$x_{i,j}^{P2} = x_{i,j} + \frac{r \cdot (u_{bj} - l_{bj})}{t}, i = 1, 2, 3, \dots, N, j = 1, 2, \dots, d, t = 1, 2, \dots, T \quad (24)$$

$$X_i = \begin{cases} X_i^{P2}, & F_i^{P2} < F_i \\ X_i, & \text{Otherwise} \end{cases} \quad (25)$$

where $X_{i,j}^{P2}$ is the updated position and F_i^{P2} is the value of objective function. Figure 3 shows the flowchart for the suggested SOA approach.

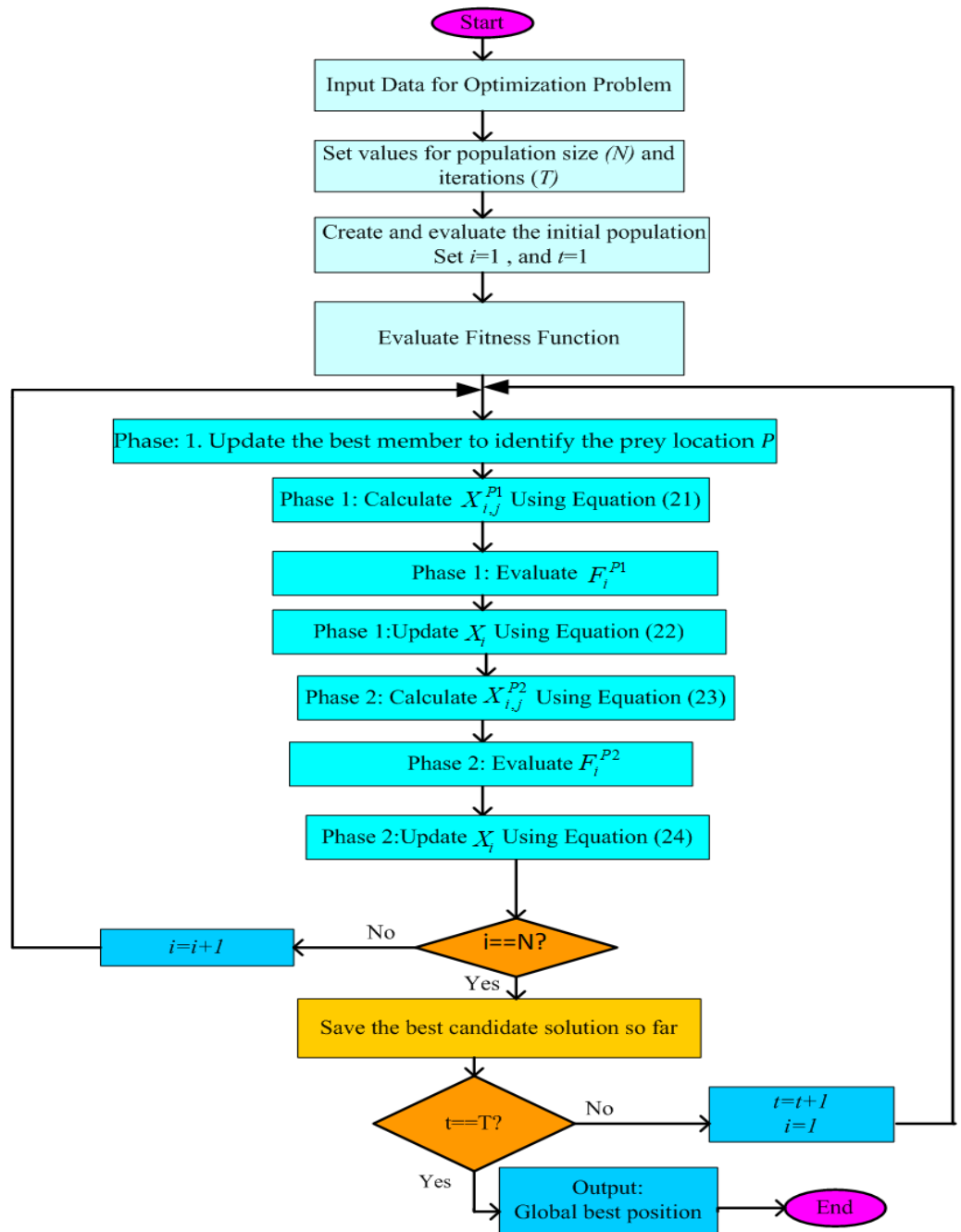


Figure 3. Flow chart of the SOA.

4. Proposed Control Techniques

Due to their simplicity and ease of implementation, PID controllers are broadly used in engineering applications. Although PID controllers perform satisfactorily in most control systems, updated PID control structures have demonstrated improved performance in a variety of control systems, including the LFC interlinked power network. In order to improve the system dynamics, the PIDF combines a PID controller with a low-pass filter applied to the derivative term. By using a low-pass filter, the oscillations caused by high-frequency oscillations can be suppressed in the system. To stabilize the frequency of the system, a PIDF controller and its modified form are developed and implemented in this work for marine microgrid systems. The proposed PIDF and I-PDF control structures are depicted in Figures 4 and 5, respectively. Similarly, the TF for the proposed PIDF and I-PDF can be found in Equations (26) and (27).

$$U(s) = \left[K_p + \frac{K_i}{s} + \frac{Ns}{N+s}K_d \right] E(s) \tag{26}$$

$$U(s) = E(s) \left[\frac{K_i}{s} \right] - Y(s) \left[K_p + \frac{Ns}{N+s}K_d \right] \tag{27}$$

where $Y(s)$, $U(s)$, $E(s)$ are the output, control, and error signals. As a result, the optimal solution to the LFC problem can be found by minimizing the cost function (J). As shown by the following equations, several performance indices—such as ISE, ITAE, and ITSE—can be utilized to reduce error signals.

$$J_{ISE} = \int_0^t (\Delta F^2) dt \tag{28}$$

$$J_{ITAE} = \int_0^t (|\Delta F|) t dt \tag{29}$$

$$J_{ITSE} = \int_0^t (|\Delta F^2|) t dt \tag{30}$$

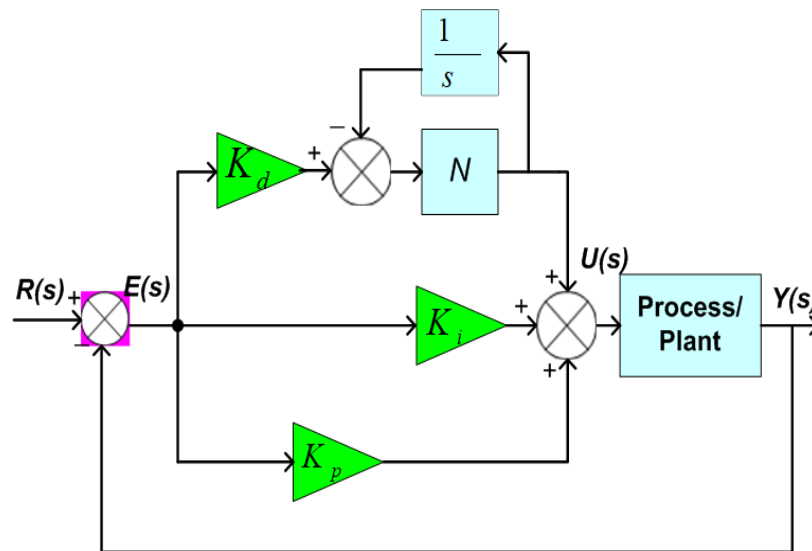


Figure 4. Configuration for PIDF controller.

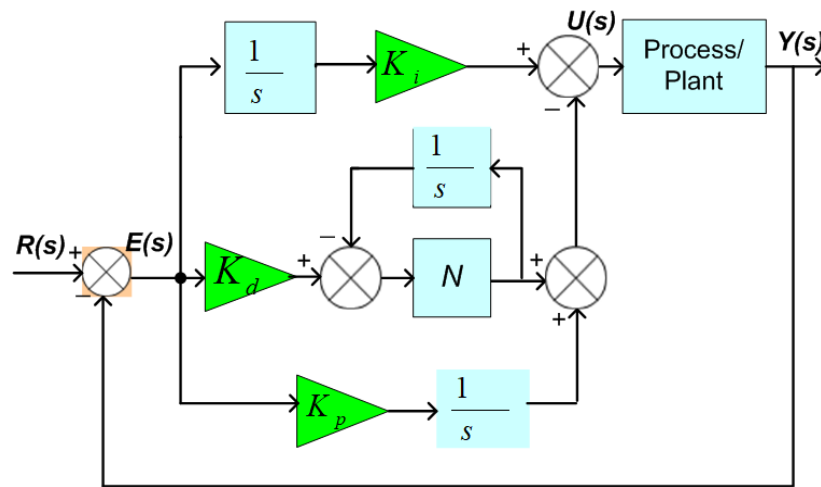


Figure 5. Configuration for the I-PDF controller.

5. Results and Discussion

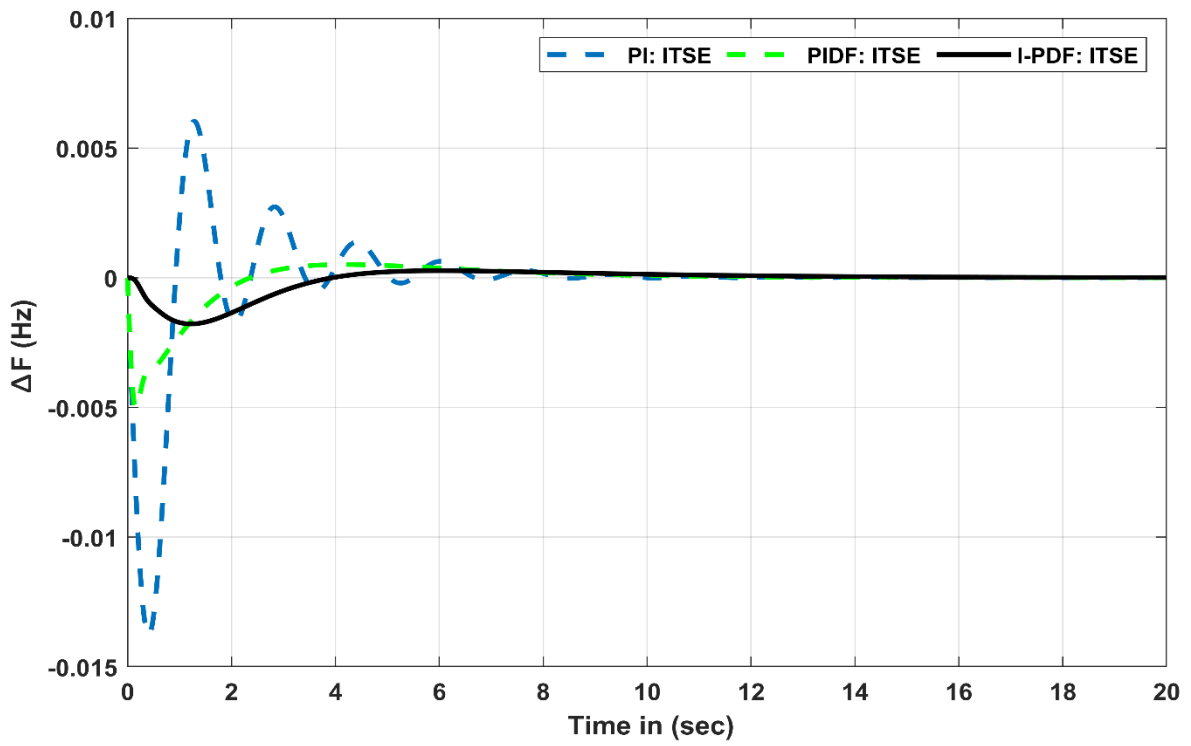
The control method was validated by simulating a maritime microgrid system in MATLAB/Simulink software (2022b). Appendix A has a list of maritime microgrid parameters. The modified PIDF controller’s performance was compared to that of the PI and PIDF controllers. Using the data in Appendix B, the SOA optimization algorithm optimized all of the parameters of these controllers, which are listed in Table 1. The proposed control mechanism was validated using real-time wind and solar emission data. The following case studies evaluate the results of the analyzed marine microgrid system.

Scenario-1 (Controllers comparison using different performance indices)

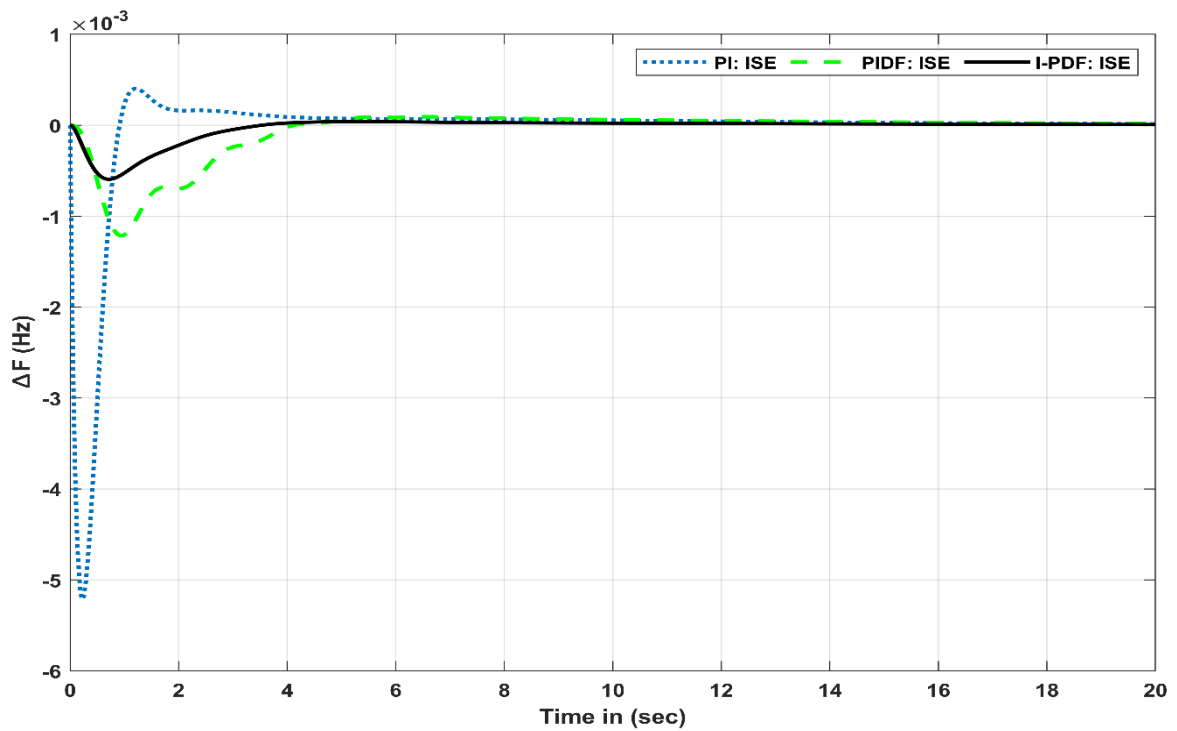
Table 1. Parametric values of proposed techniques.

Controller Gains	I-PDF	PIDF	PI	SOA	JSO	ACO	PSO
K_p	19.11	10.18	09.98	19.40	13.20	13.08	11.23
K_i	11.91	18.86	18.01	17.13	05.02	23.10	11.98
K_d	12.56	14.07	11.90	09.10	10.20	14.78	19.11
N	56.89	45.01	-	98.78	34.09	51.01	98.30

This study compared the efficiency of an I-PDF controller with the performance of PI and PIDF controllers based on a number of different multi-objective cost performance indices, including ITSE, ISE, and ITAE. The dynamic response of each controller, as shown in Figure 6a–c, was evaluated with respect to a number of multi-objective cost performance indices—such as ITSE, ISE, and ITAE—in order to determine the controller’s performance over time. The undershoot (Ush), settling time (ST), and overshoot (Osh) for the ITSE, ISE, and ITAE criteria are compared in Table 2. The I-PDF controller—which was tuned using the SOA method—virtually had the same peak overshoot as the PIDF controller, but it improved the ST for the ITAE and ISE by 29.10% and 52.82%, respectively, compared to the PIDF controller. As shown in Table 2, I-PDF controllers have better performance than PIDF controllers in terms of ST and Ush when applied to the ITSE, ISE, and ITAE, where ST is improved by 51.11%, 34.09%, and 19.05%, respectively, and Ush is improved by 89.00%, 78.13%, and 91.20%. In addition, we found that our recommended I-PDF controller reduced peak overshoot by 64.09%, 59.51%, and 81.55% in comparison to a PI controller, undershoot by 91.22%, 83.44%, and 56.78%, and settling time by 56.46%, 34.56%, and 29.87%, respectively, for the ITSE, ISE, and ITAE. In Table 2, all of the performance parameters were clearly shown to be outperformed by the proposed control strategies when compared to PI and PIDF controllers. The best results are bolded in Table 2.



(a)



(b)

Figure 6. Cont.

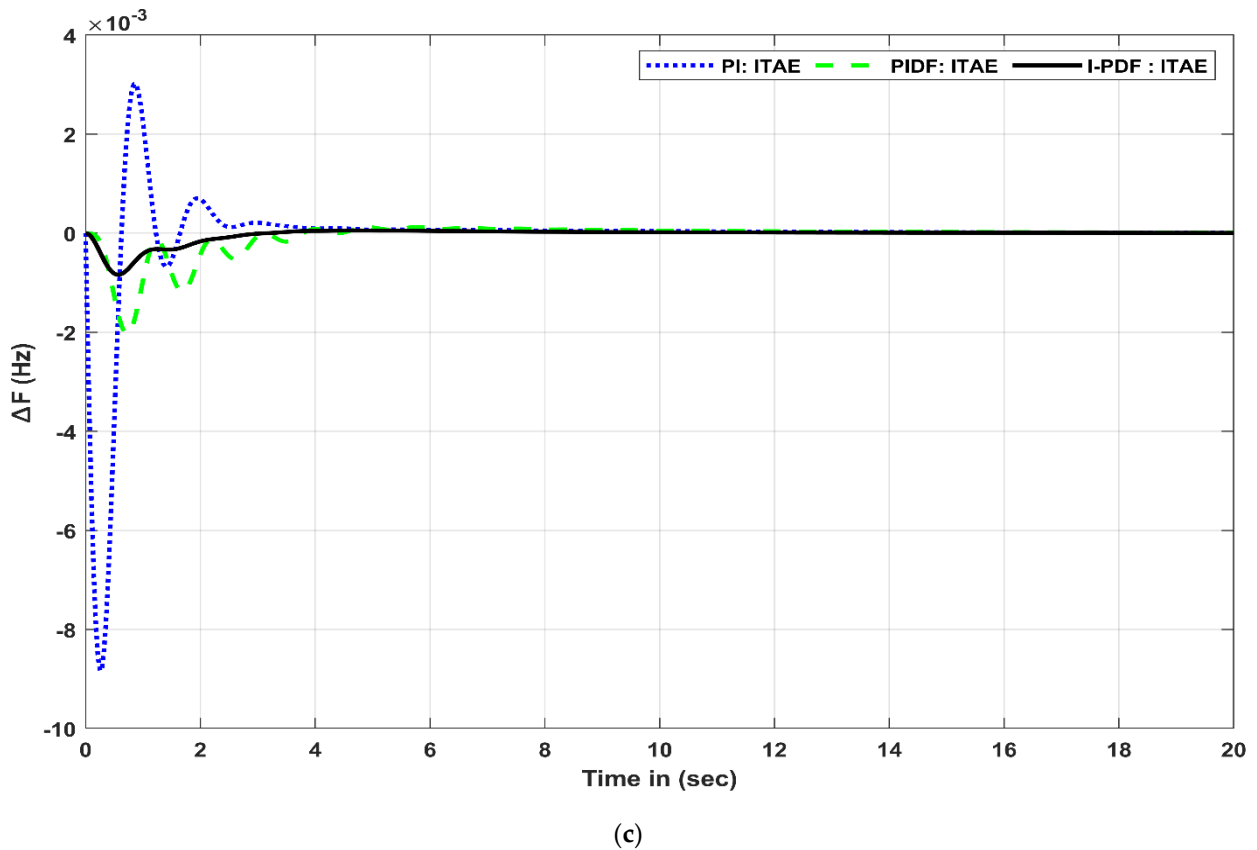


Figure 6. Dynamic response of the marine microgrid system for scenario1 (a) ITSE (b) ISE (c) ITAE.

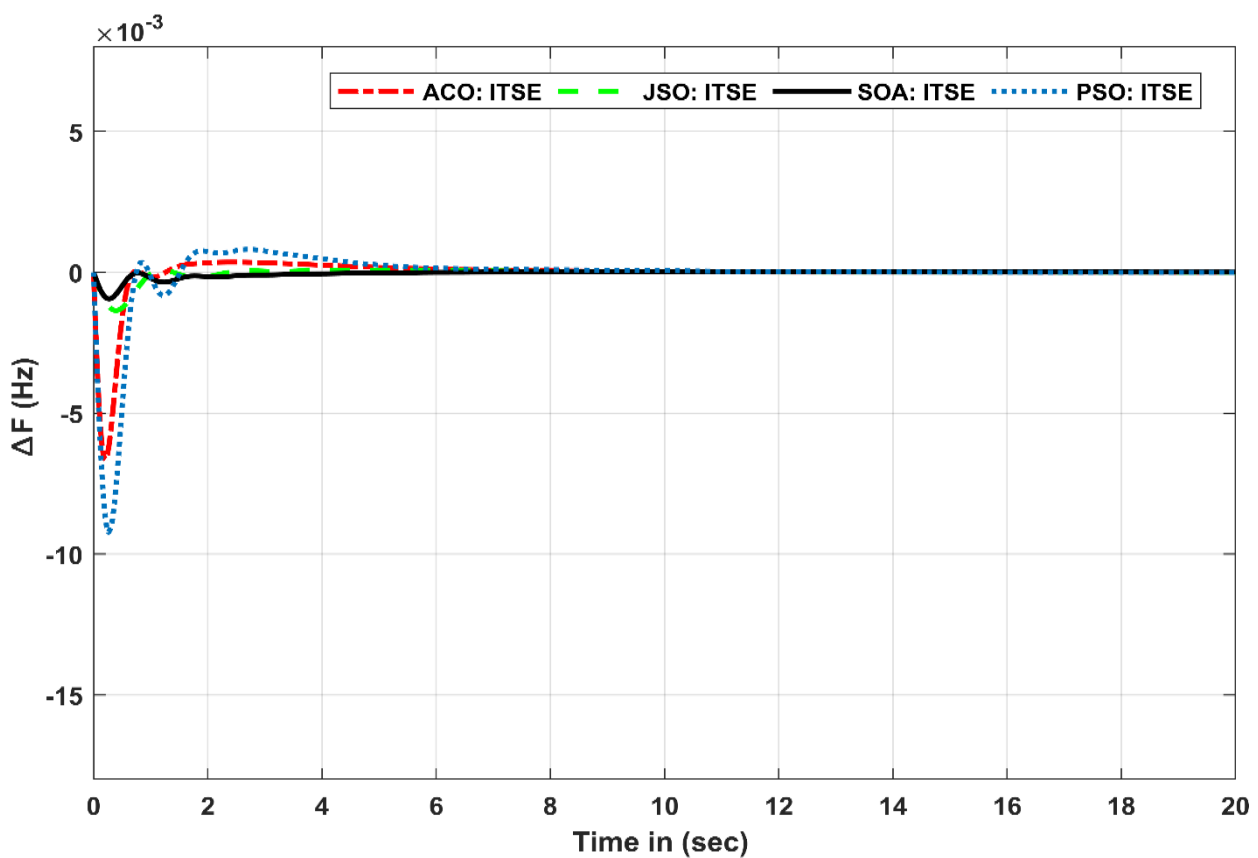
Table 2. Comparison performance of various controllers using different performance indices.

Transient Parameters	Performance Indices	PI Controller	PIDF Controller	I-PDF Controller
Time Settling (ST)	ITSE	05.91	08.09	03.93
	ISE	10.40	08.46	08.23
	ITAE	04.68	07.83	02.96
Overshoot (O_{sh})	ITSE	0.00040	0.00009	0.00004
	ISE	0.00603	0.00050	0.00027
	ITAE	0.00301	0.00012	0.00000
Undershoot (U_{sh})	ITSE	-0.00521	-0.00121	-0.00059
	ISE	-0.01376	-0.00500	-0.00178
	ITAE	-0.00883	-0.00202	-0.00084

Scenario-2 (Comparison of algorithms based on performance indices)

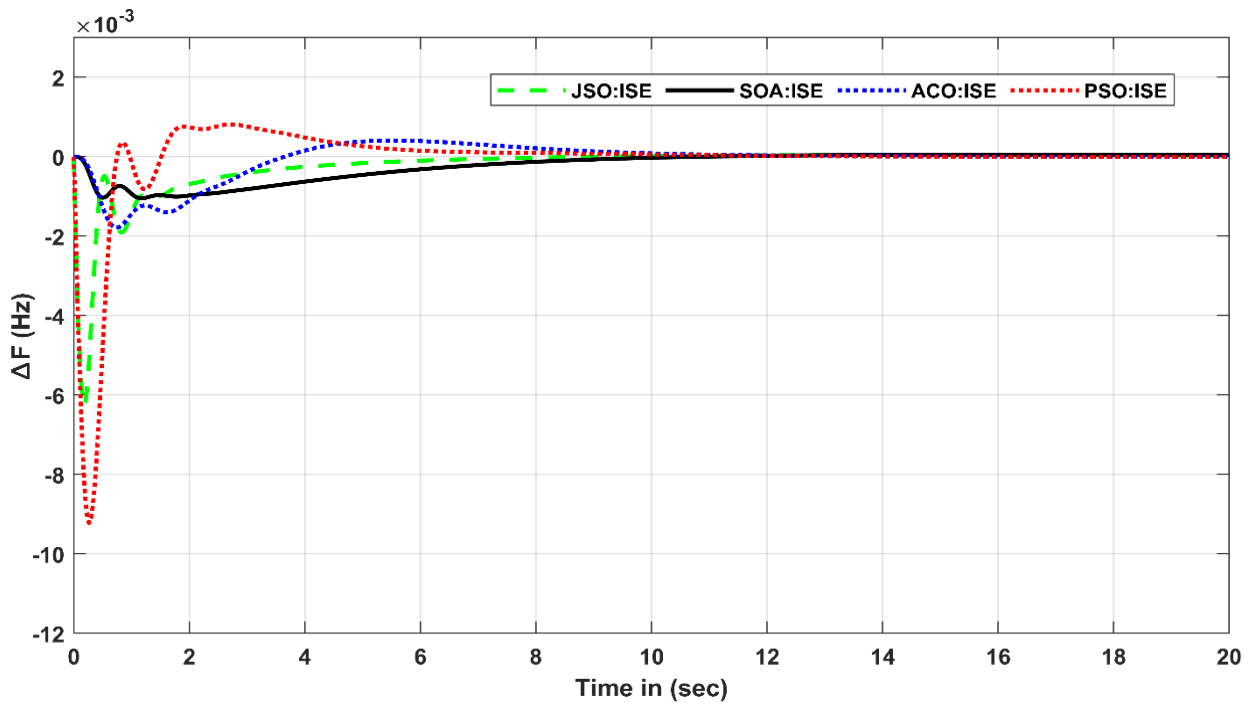
In this study, we compared the jellyfish swarm optimization (JSO), the ant colony optimization (ACO), and the particle swarm optimization (PSO) algorithms with our proposed serval optimization algorithm (SOA). Figure 7a–c illustrates the dynamic response of the different algorithms to several multi-objective cost performance indicators, including ITSE, ISE, and ITAE. A comparison of different algorithms for transitory content—such as O_{sh} , U_{sh} , and ST for ITSE, ISE, and ITAE—is presented in Table 3. Table 3 and Figure 7a–c indicate that our recommended metaheuristic algorithms achieve better performance for U_{sh} and O_{sh} for ITSE, ISE, and ITAE, when compared to JSO, ACO, and PSO, respectively. In Table 3, it can be seen that our proposed SOA algorithm ($U_{sh} = -0.00065$, $O_{sh} = 0.000129$) had less

undershoot and overshoot when compared with PSO (Ush = -0.00722, Osh= 0.001045), JSO (Ush = -0.00119, Osh = 0.000218), and ACO (Ush = -0.00628, Osh= 0.000437). According to Table 3, particle swarm optimization had the lowest settling time for the ITAE (ST = 5.98 s). The serval optimization algorithm (SOA) had the second lowest settling time for the ITAE (ST = 6.72 s), followed by jellyfish swarm optimization (JSO) with an ST of 8.83 s, and ant colony optimization with an ST of 12.60 s. The SOA algorithm (ST = 4.420 s) also outperformed existing algorithms such as JSO (ST = 5.02 s), PSO (ST = 8.89 s) and ACO (ST = 6.533 s) for the ITSE objective criterion in a similar manner. In addition to taking into account transient response criteria, we also found that our suggested SOA algorithm performed admirably when compared to other competing algorithms such as JSO, PSO, and ACO when considering ISE cost function indices. As shown in Table 3 and Figure 7a–c, the current methodology outperformed JSO, PSO, and ACO in terms of ST, Osh, and Ush for the ITSE, ISE and ITAE performance indices. The best results are bolded in Table 3.

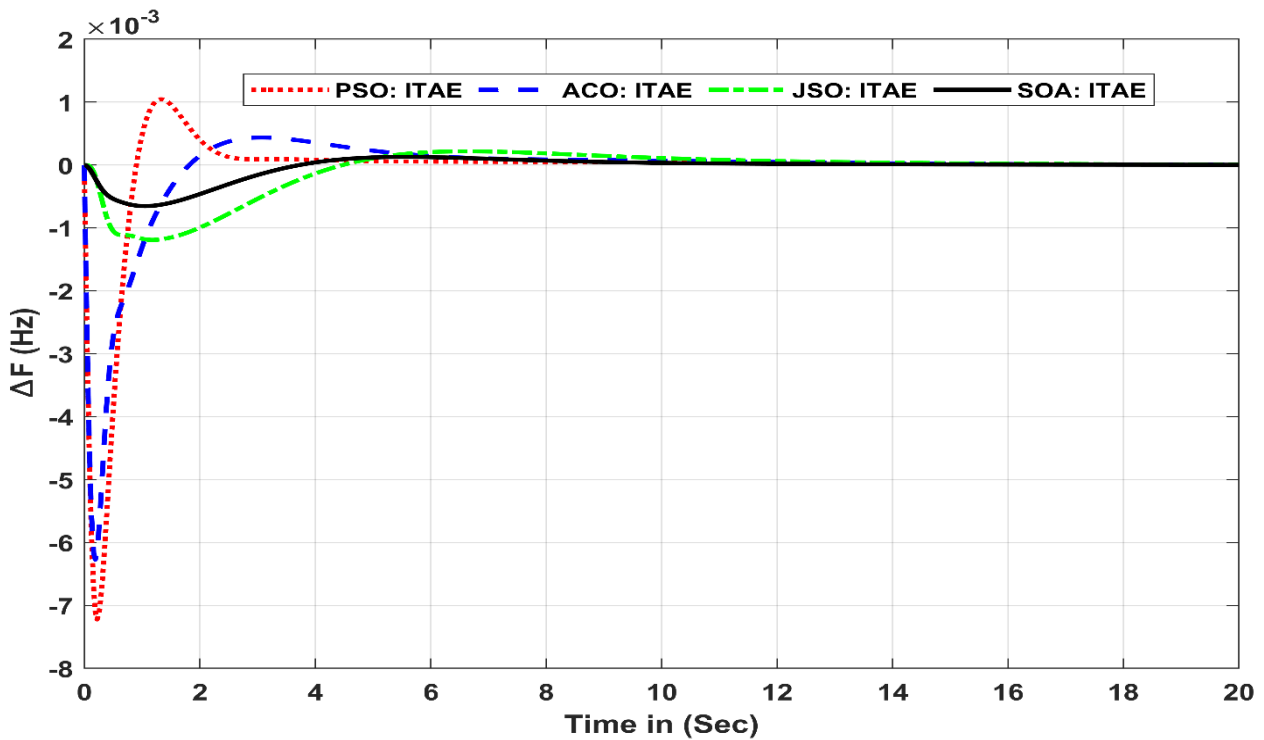


(a)

Figure 7. Cont.



(b)



(c)

Figure 7. Dynamic response of the Marine Microgrid system for scenario-2 (a) ITSE (b) ISE (c) ITAE.

Scenario-3 (Sensitivity and Robustness)

Under various loading disturbances, this scenario tested the resilience of the proposed SOA-based I-PDF controller. Figure 8 shows the frequency oscillations that took place when the load was changed, along with the different controllers utilized for it. From Figure 8, it can be noticed that the SOA-based I-PDF controller provided the best response to random

load variations compared to the SOA-based PIDF and PI controllers. Compared to other controllers, our proposed controller achieved less steady-state errors, faster responses, and superior damped variation on a continuous basis. Furthermore, different load interruptions fluctuating from $\pm 25\%$ to $\pm 50\%$ were applied to a marine microgrid system in order to check the robustness of the proposed control scheme that was developed, and the results are shown in Figure 9 for comparison. The results clearly demonstrated that the proposed controller was able to produce the same fault-tolerance performance even when the load was varied from $\pm 25\%$ to $\pm 50\%$. This clearly shows the robustness of our proposed controller. A sensitivity assessment was conducted by varying K_{PV} , R , and K_{wave} by $\pm 30\%$ in order to test the robustness of the proposed SOA-based I-PDF controller. The dynamic responses of the model are illustrated in Figure 10 for the purpose of the above sensitivity assessment. Under uncertain conditions, the system dynamics will not deviate significantly from their base conditions, as shown in Figure 10. In Table 4, the transient response of various parameters is shown up to a $\pm 30\%$ change in parametric values. Finally, it was found that the parameters of the tuned I-PDF controller were quite robust to uncertainty as well as parametric variations of the proposed marine microgrid.

Table 3. Comparison performance of different algorithms using different performance indices.

Transient Response	Performance Indices	ACO Algorithm	PSO Algorithm	JSO Algorithm	SOA Algorithm
Time Settling (ST)	ITSE	08.43	06.53	05.02	04.42
	ISE	10.90	08.61	06.23	09.93
	ITAE	05.98	08.83	12.60	06.82
Overshoot (O_{sh})	ITSE	0.00081	0.00036	0.00008	0.00001
	ISE	0.00081	0.00040	0.0000437	0.00004
	ITAE	0.001045	0.00043	0.0002180	0.00012
Undershoot (U_{sh})	ITSE	-0.00922	-0.00664	-0.00135	-0.00094
	ISE	-0.00921	-0.00179	-0.00628	-0.00104
	ITAE	-0.00722	0.006270	-0.00119	-0.00065

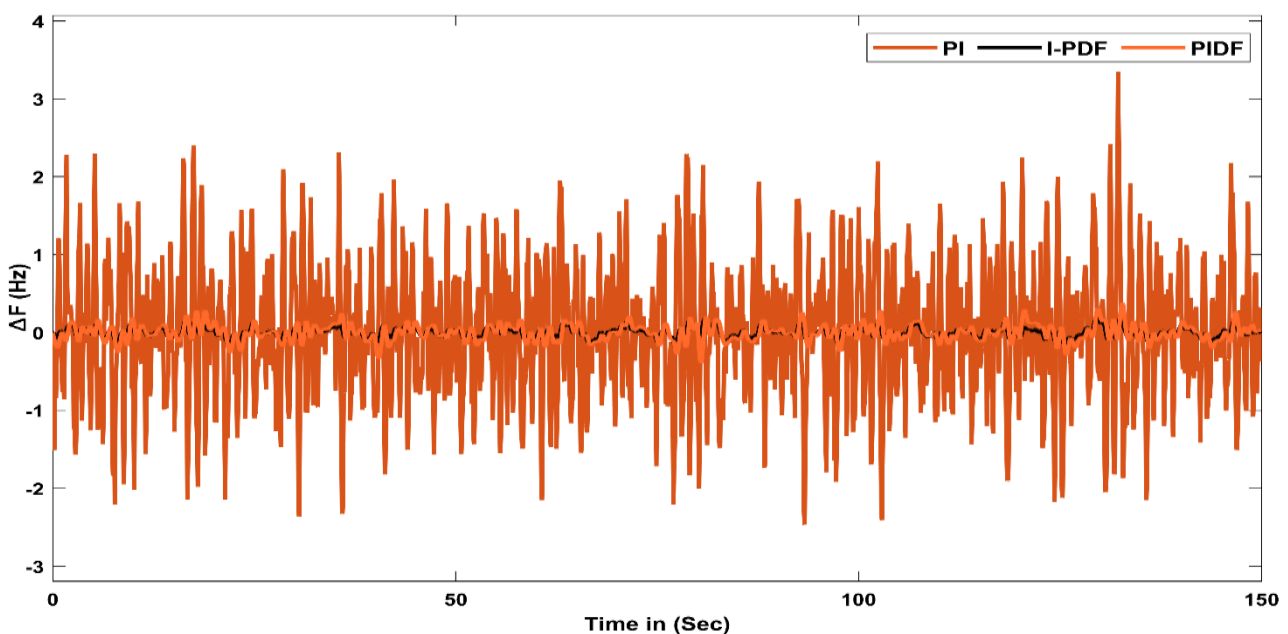


Figure 8. Random load frequency variation of the marine microgrid system.

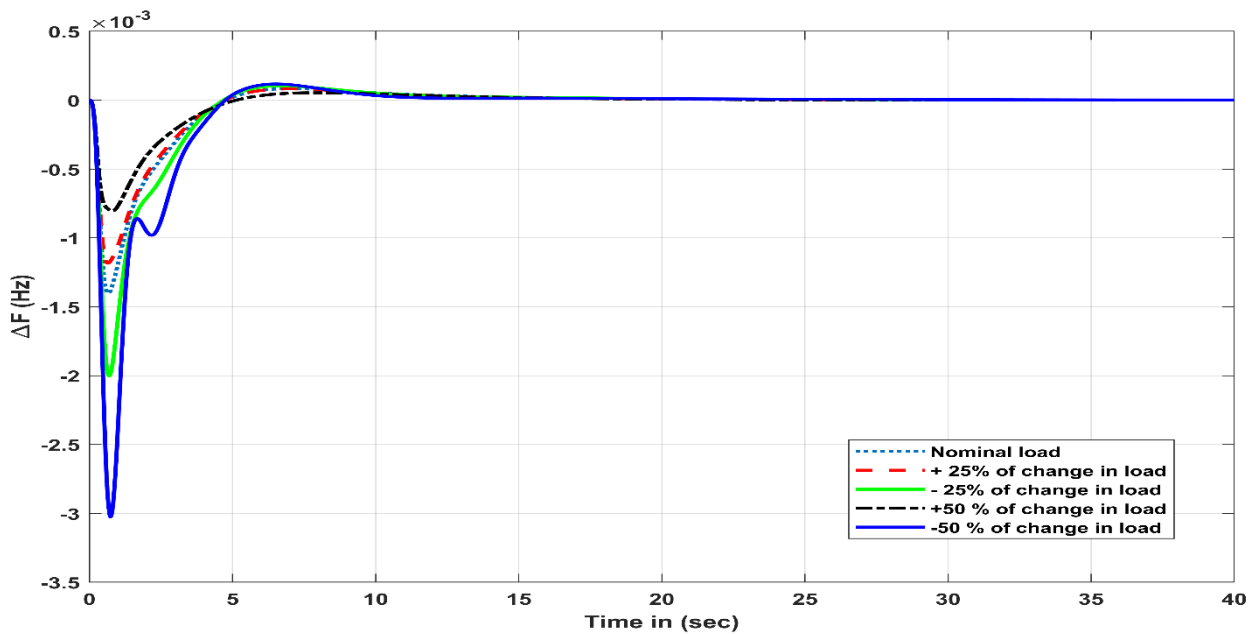


Figure 9. Load variation for the marine microgrid system from ±25% to ±50%.

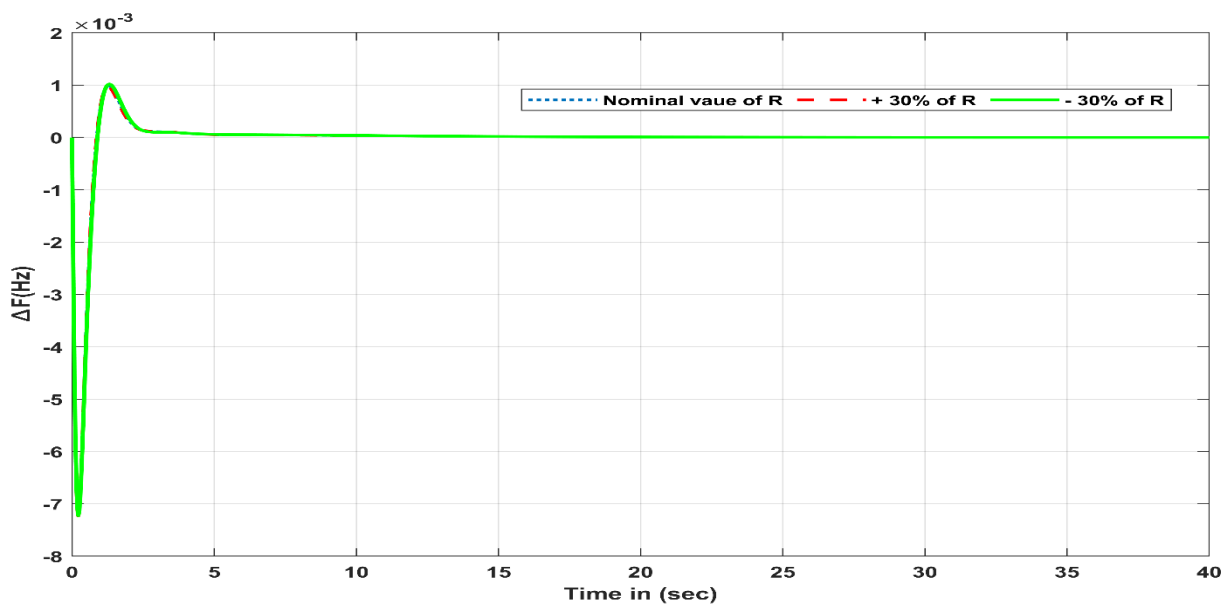


Figure 10. Parametric variation in R.

Table 4. Sensitivity analysis for changes in parameters of the power system with various performance indices.

Transient Terms	Power System Parameters	% Change	ITAE	ITSE	ISE
Time Settling (ST)	K_{wave}	+30	14.09	3.47	12.72
		-30	14.10	3.51	12.73
	R	+30	14.21	6.38	13.45
		-30	14.23	8.03	13.46
	K_{PV}	+30	14.60	6.10	12.79
		-30	14.61	7.80	12.80

Table 4. *Cont.*

Transient Terms	Power System Parameters	% Change	ITAE	ITSE	ISE
Overshoot (O _{sh})	K _{wave}	+30	0.00064	0.000323	0.00068
		−30	0.00054	0.000276	0.00047
	R	+30	0.00094	0.000296	0.00037
		−30	0.00098	0.000289	0.00030
	K _{PV}	+30	0.00083	0.000310	0.00014
		−30	0.00075	0.000313	0.00017
Undershoot (U _{sh})	K _{wave}	+30	−0.00610	−0.00315	−0.00240
		−30	−0.00600	−0.00313	−0.00236
	R	+30	−0.00693	−0.00489	−0.00713
		−30	−0.00678	−0.00482	−0.00913
	K _{PV}	+30	−0.00731	−0.00361	−0.00780
		−30	−0.00725	−0.00361	−0.00740

6. Conclusions and Future Recommendations

In this study, an innovative controller and optimization methodology were developed for LFCs in a marine microgrid system with renewable energy sources. A modified PIDF controller, known as the I-PDF controller, was implemented in this study in order to establish the dynamics of the system and compare them with various case studies. Furthermore, the novel aspect of this work was the application of a newly developed serval optimization algorithm (SOA) to tune the modified PID controller based on real-time wind data at the time of tuning. It has been found that SOA-tuned I-PDF controllers perform better than algorithmically tuned I-PDF controllers in terms of U_{sh}, ST, and O_{sh}. This study validates the superiority of the proposed I-PDF controller compared with other controllers based on the statistical performance evaluation. Our proposed I-PDF controllers showed better performance than PIDF controllers in terms of ST and U_{sh} when applied to ITSE, ISE, and ITAE, where ST was improved by 51.11%, 34.09%, and 19.05%, respectively, and U_{sh} was improved by 89.00%, 78.13%, and 91.20%. Finally, SOA-based I-PDF controller parameters were found to be very robust to uncertainty/parametric variation for marine microgrids. In future, the proposed control scheme and other advanced controllers such as FLCs and MPCs may be designed and implemented in Matlab/Simulink, as well as the practical use of OPAL-RT simulators for marine microgrids, with the inclusion of renewable energies and energy storage devices.

Author Contributions: Conceptualization, G.Z.; Data curation, A.B.; Formal analysis, A.B. and M.I.K.; Funding acquisition, M.I.K.; Investigation, G.Z., A.D. and M.I.K.; Methodology, A.D. and M.I.K.; Project administration, G.Z.; Resources, I.A.K.; Software, I.A.K. and A.B.; Supervision, G.Z.; Validation, G.Z. and I.A.K.; Visualization, I.A.K.; Writing—original draft, A.D.; Writing—review and editing, A.B. All authors have read and agreed to the published version of the manuscript.

Funding: This work is supported by “Young Talent Sub-project of Ningbo Yongjiang Talent Introduction Programme under grant no 20100859001”.

Institutional Review Board Statement: Not applicable.

Informed Consent Statement: Not applicable.

Conflicts of Interest: The authors declare no conflict of interest.

Abbreviations

Acronym	Definition	Acronym	Definition
WTB	Wind Turbine Generator	RES	Renewable Energy Sources
LFC	Load Frequency Control	SLP	Step Load Perturbation
SOA	Serval Optimization Algorithm	SWE	Sea wave energy
ACO	Ant Colony Optimization	ΔF	Frequency Deviation
IPS	Interconnected Power System	PID	Proportional Integral Derivative
GHG	Green House Gases	PSO	Particle Swarm Optimization
JSO	Jellyfish Swarm Optimization	ABC	Artificial Bee Colony
PD	Proportional Derivative	MMS	Marine Microgrid System
PV	Photo Voltaic	PS	Power System
B	Area Bias Factor	PI	Proportional Integral
WT	Wind Turbine	SWE	Sea Wave Energy
HPS	Hybrid Power System	IMO	International Maritime Organization
ΔP_D	Load Deviation	MG	Microgrid
R	Speed Regulation	HMG	Hybrid Microgrid
ΔP_G	Deviation in the Output of Generator	ΔX_G	Valve Position of Governor
ANN	Artificial Neural networks	FLC	Fuzzy Logic Control
K_{pv}	Photovoltaic Constant	TIDN	Tilt integral derivative with filter
ST	Settling time	T_w	Wind Time Constant
U_{sh}	Undershoot	LB	Lower Boundary
PID	Proportional-Integral-Derivative	K_{wave}	Gain of wave energy
T_p	Time Constant of Power System	TD	Time Delay
O_{sh}	Overshoot	TF	Transfer Function
ISE	Integral Square Error	FO	Fractional Order
M	Inertia Constant	PIDF	Proportional Integral Derivative with Filter
H	Power System Gain	UB	Upper Boundary
ITAE	Integral Time Absolute Error	ITSE	Integral Time Square Error

Appendix A. Hybrid PS and Their Parametric Values [25,27,31]

LFC Model			
Parameter	Value	Parameter	Value
T_g	2 S	T_G	0.5 s
R	2.4 (pu.Mw/s)	2 H	0.2 (p.u.·s)
T_{ps2}	11.49	D	0.012 (p.u./Hz)
T_h	5 S	Tcon	0.5 S
T_{in}	4 S	T_{FESS}	0.1 S
K_{VR}	1	T_{BESS}	0.1 S
T_{VR}	0.08 S	R	0.5 m
H	2 m	K_{BE}	1
T_{CE}	0.4 S	K_{wave}	1
T_{wave}	5 S	C_p	0.195
J_G	1.53 km·m ²	D	628 m
K_s	0.5	K_T	1
T_s	1	T_T	0.3
K_{WTG}	1	T_{WTG}	1.5
K_{PV}	1		

Appendix B. SOA Coefficient and Their Values

Parameters of SOA Algorithm	Values	Parameters of SOA Algorithm	Values
No. of Iterations	100	Lower limit (Lb)	−2
No. of Population (Np)	30	Constant (R)	0.05
No. of dimensions	4	Coefficient (a)	2
Random Number (r)	[0, 1]		

References

- Iris, Ç.; Lam, J.S.L. A review of energy efficiency in ports: Operational strategies, technologies and energy management systems. *Renew. Sustain. Energy Rev.* **2019**, *112*, 170–182. [[CrossRef](#)]
- Shariatzadeh, F.; Kumar, N.; Srivastava, A.K. Optimal Control Algorithms for Reconfiguration of Shipboard Microgrid Distribution System Using Intelligent Techniques. *IEEE Trans. Ind. Appl.* **2017**, *53*, 474–482. [[CrossRef](#)]
- Maleki, A.; Askarzadeh, A. Optimal sizing of a PV/wind/diesel system with battery storage for electrification to an off-grid remote region: A case study of Rafsanjan, Iran. *Sustain. Energy Technol. Assess.* **2014**, *7*, 147–153. [[CrossRef](#)]
- Rourke, F.O.; Boyle, F.; Reynolds, A. Tidal energy update 2009. *Appl. Energy* **2010**, *87*, 398–409. [[CrossRef](#)]
- Ovrum, E.; Bergh, T. Modelling lithium-ion battery hybrid ship crane operation. *Appl. Energy* **2015**, *152*, 162–172. [[CrossRef](#)]
- Whitby, B.; Ugalde-Loo, C.E. Performance of Pitch and Stall Regulated Tidal Stream Turbines. *IEEE Trans. Sustain. Energy* **2013**, *5*, 64–72. [[CrossRef](#)]
- Maleki, A.; Askarzadeh, A. Artificial bee swarm optimization for optimum sizing of a stand-alone PV/WT/FC hybrid system considering LPSP concept. *Sol. Energy* **2014**, *107*, 227–235. [[CrossRef](#)]
- Jin, Z.; Sulligoi, G.; Cuzner, R.; Meng, L.; Vasquez, J.C.; Guerrero, J.M. Next-generation shipboard DC power system: Introduction smart grid and DC microgrid technologies into maritime electrical networks. *IEEE Electr. Mag.* **2016**, *4*, 45–57. [[CrossRef](#)]
- Geertsma, R.D.; Negenborn, R.R.; Visser, K.; Hopman, J.J. Design and control of hybrid power and propulsion systems for smart ships: A review of developments. *Appl. Energy* **2017**, *194*, 34–54. [[CrossRef](#)]
- Iris, Ç.; Lam, J.S.L. Optimal energy management and operations planning in seaports with smart grid while harnessing renewable energy under uncertainty. *Omega* **2021**, *103*, 102445. [[CrossRef](#)]
- Wen, S.; Lan, H.; Hong, Y.-Y.; Yu, D.C.; Zhang, L.; Cheng, P. Allocation of ESS by interval optimization method considering impact of ship swinging on hybrid PV/diesel ship power system. *Appl. Energy* **2016**, *175*, 158–167. [[CrossRef](#)]
- Bryans, A.; Fox, B.; Crossley, P.; O'Malley, M. Impact of Tidal Generation on Power System Operation in Ireland. *IEEE Trans. Power Syst.* **2005**, *20*, 2034–2040. [[CrossRef](#)]
- Mauricio, J.M.; Marano, A.; Gomez-Exposito, A.; Ramos, J.L.M. Frequency Regulation Contribution through Variable-Speed Wind Energy Conversion Systems. *IEEE Trans. Power Syst.* **2009**, *24*, 173–180. [[CrossRef](#)]
- Huang, J.; Yang, J.; Xie, D.; Wu, D. Optimal Sliding Mode Chaos Control of Direct-Drive Wave Power Converter. *IEEE Access* **2019**, *7*, 90922–90930. [[CrossRef](#)]
- Hasanien, H.M. Transient Stability Augmentation of a Wave Energy Conversion System Using a Water Cycle Algorithm-Based Multiobjective Optimal Control Strategy. *IEEE Trans. Ind. Inform.* **2018**, *15*, 3411–3419. [[CrossRef](#)]
- González, I.; Calderón, A.J.; Folgado, F.J. IoT real time system for monitoring lithium-ion battery long-term operation in microgrids. *J. Energy Storage* **2022**, *51*, 104596. [[CrossRef](#)]
- Jha, A.V.; Gupta, D.K.; Appasani, B. The PI Controllers and its optimal tuning for Load Frequency Control (LFC) of Hybrid Hydro-thermal Power Systems. In Proceedings of the 2019 International Conference on Communication and Electronics Systems, Coimbatore, India, 17–19 July 2019; pp. 1866–1870. [[CrossRef](#)]
- Ali, T.; Malik, S.A.; Daraz, A.; Aslam, S.; Alkhalifah, T. Dandelion Optimizer-Based Combined Automatic Volt-age Regulation and Load Frequency Control in a Multi-Area, Multi-Source Interconnected Power System with nonlinearities. *Energies* **2022**, *15*, 8499. [[CrossRef](#)]
- Dhillon, S.S.; Lather, J.; Marwaha, S. Multi objective load frequency control using hybrid bacterial foraging and particle swarm optimized PI controller. *Int. J. Electr. Power Energy Syst.* **2016**, *79*, 196–209. [[CrossRef](#)]
- Alayi, R.; Zishan, F.; Seyednouri, S.R.; Kumar, R.; Ahmadi, M.H.; Sharifpur, M. Optimal Load Frequency Control of Island Microgrids via a PID Controller in the Presence of Wind Turbine and PV. *Sustainability* **2021**, *13*, 10728. [[CrossRef](#)]
- Coban, H.H.; Rehman, A.; Mousa, M. Load Frequency Control of Microgrid System by Battery and Pumped-Hydro Energy Storage. *Water* **2022**, *14*, 1818. [[CrossRef](#)]
- Daraz, A.; Malik, S.A.; Mokhlis, H.; Haq, I.U.; Laghari, G.F.; Mansor, N.N. Fitness Dependent Optimizer-Based Automatic Generation Control of Multi-Source Interconnected Power System With Non-Linearities. *IEEE Access* **2020**, *8*, 100989–101003. [[CrossRef](#)]
- Chen, G.; Li, Z.; Zhang, Z.; Li, S. An Improved ACO Algorithm Optimized Fuzzy PID Controller for Load Frequency Control in Multi Area Interconnected Power Systems. *IEEE Access* **2020**, *8*, 6429–6447. [[CrossRef](#)]

24. Sariki, M.; Shankar, R. Optimal CC-2DOF(PI)-PDF controller for LFC of restructured multi-area power system with IES-based modified HVDC tie-line and electric vehicles. *Eng. Sci. Technol. Int. J.* **2022**, *32*, 101058. [[CrossRef](#)]
25. Zhang, P.; Daraz, A.; Malik, S.A.; Sun, C.; Basit, A.; Zhang, G. Multi-resolution based PID controller for frequency regulation of a hybrid power system with multiple interconnected systems. *Front. Energy Res.* **2023**, *10*, 1109063. [[CrossRef](#)]
26. Prakash, A.; Kumar, K.; Parida, S.K. PIDF(1 + FOD) controller for load frequency control with SSSC and AC–DC tie-line in deregulated environment. *IET Gener. Transm. Distrib.* **2020**, *14*, 2751–2762. [[CrossRef](#)]
27. Hasanien, H.M. Whale optimisation algorithm for automatic generation control of interconnected modern power systems including renewable energy sources. *IET Gener. Transm. Distrib.* **2018**, *12*, 607–614. [[CrossRef](#)]
28. Daraz, A.; Malik, S.A.; Mokhlis, H.; Haq, I.U.; Zafar, F.; Mansor, N.N. Improved-Fitness Dependent Optimizer Based FOI-PD Controller for Automatic Generation Control of Multi-Source Interconnected Power System in Deregulated Environment. *IEEE Access* **2020**, *8*, 197757–197775. [[CrossRef](#)]
29. El-Fergany, A.A.; El-Hameed, M.A. Efficient frequency controllers for autonomous two-area hybrid microgrid system using social-spider optimiser. *IET Gener. Transm. Distrib.* **2017**, *11*, 637–648. [[CrossRef](#)]
30. Shayeghi, H.; Rahnama, A.; Mohajery, R.; Bizon, N.; Mazare, A.G.; Ionescu, L.M. Multi-Area Microgrid Load-Frequency Control Using Combined Fractional and Integer Order Master–Slave Controller Considering Electric Vehicle Aggregator Effects. *Electronics* **2022**, *11*, 3440. [[CrossRef](#)]
31. Daraz, A.; Malik, S.A.; Basit, A.; Aslam, S.; Zhang, G. Modified FOPID Controller for Frequency Regulation of a Hybrid Interconnected System of Conventional and Renewable Energy Sources. *Fractal Fract.* **2023**, *7*, 89. [[CrossRef](#)]
32. Fathy, A.; Kassem, A.M. Antlion optimizer-ANFIS load frequency control for multi-interconnected plants comprising photovoltaic and wind turbine. *ISA Trans.* **2019**, *87*, 282–296. [[CrossRef](#)] [[PubMed](#)]
33. Wu, T.; Zhou, C.; Yan, Z.; Peng, H.; Wu, L. Application of PID optimization control strategy based on particle swarm optimization (PSO) for battery charging system. *Int. J. Low Carbon Technol.* **2020**, *15*, 528–535. [[CrossRef](#)]
34. Daraz, A.; Malik, S.A.; Azar, A.T.; Aslam, S.; Alkhalifah, T.; Alturise, F. Optimized Fractional Order Integral-Tilt Derivative Controller for Frequency Regulation of Interconnected Diverse Renewable Energy Resources. *IEEE Access* **2022**, *10*, 43514–43527. [[CrossRef](#)]
35. Cuoghi, S.; Ntogramatzidis, L.; Padula, F.; Grandi, G. Direct Digital Design of PIDF Controllers with Complex Zeros for DC-DC Buck Converters. *Energies* **2018**, *12*, 36. [[CrossRef](#)]
36. Siddiqui, M.A.; Anwar, N.; Laskar, S.H. Tuning of PIDF Controller in Parallel Control Structure for Integrating Process with Time Delay and Inverse Response Characteristic. *J. Control. Autom. Electr. Syst.* **2020**, *31*, 829–841. [[CrossRef](#)]
37. Lamba, R.; Singla, S.K.; Sondhi, S. Design of Fractional Order PID Controller for Load Frequency Control in Perturbed Two Area Interconnected System. *Electr. Power Compon. Syst.* **2019**, *47*, 998–1011. [[CrossRef](#)]
38. Daraz, A.; Malik, S.A.; Waseem, A.; Azar, A.T.; Haq, I.U.; Ullah, Z.; Aslam, S. Automatic Generation Control of Multi-Source Interconnected Power System Using FOI-TD Controller. *Energies* **2021**, *14*, 5867. [[CrossRef](#)]
39. Katawaluwa, M.; Zhang, H.; Vagapov, Y.; Evans, J. Simulation of Wind Heat Generator. In Proceedings of the 2006 IEEE International Conference on Electro/Information Technology, East Lansing, MI, USA, 7–10 May 2006; pp. 479–482. [[CrossRef](#)]
40. Latif, A.; Hussain, S.M.S.; Das, D.C.; Ustun, T.S. Double stage controller optimization for load frequency stabilization in hybrid wind-ocean wave energy based maritime microgrid system. *Appl. Energy* **2021**, *282*, 116171. [[CrossRef](#)]
41. Khooban, M.-H.; Niknam, T.; Blaabjerg, F.; Davari, P.; Dragicevic, T. A robust adaptive load frequency control for micro-grids. *ISA Trans.* **2016**, *65*, 220–229. [[CrossRef](#)]
42. Dehghani, M.; Trojovský, P. Serval Optimization Algorithm: A New Bio-Inspired Approach for Solving Optimization Problems. *Biomimetics* **2022**, *7*, 204. [[CrossRef](#)]

Disclaimer/Publisher’s Note: The statements, opinions and data contained in all publications are solely those of the individual author(s) and contributor(s) and not of MDPI and/or the editor(s). MDPI and/or the editor(s) disclaim responsibility for any injury to people or property resulting from any ideas, methods, instructions or products referred to in the content.